

Pham Thi Nam, Nguyen Thi Thom, Nguyen Thu Phuong, Vo Thi Hanh, Nguyen Thi Thu Trang, Vu Thi Hai Van, Trinh Hoang Trung, Tran Dai Lam and Dinh Thi Mai Thanh\*

# Electrodeposition of sustainable fluoridated hydroxyapatite coatings on 316L stainless steel for application in bone implant

DOI 10.1515/gps-2016-0064

Received April 14, 2016; accepted June 27, 2016; previously published online September 21, 2016

**Abstract:** Fluoridated hydroxyapatite (FHAp) coatings were deposited on 316L stainless steel (316LSS) substrate by the electrodeposition method. Different concentrations of  $F^-$  ion were incorporated into the apatite structure by adding NaF into the electrolyte solution. The coating was uniform and dense, with thickness of 9.6  $\mu\text{m}$ , and  $F^-$  ions were doped on HAp with mass percentage of 1.7%;  $F^-$  concentration was 0.002 M. Results of IR, energy-dispersive X-ray (EDX), X-ray and scanning electron microscopy (SEM) analysis showed that the obtained coatings were single phase crystals of HAp, of a cylinder shape with average size of about 100 nm $\times$ 30 nm, and characterized for the molecular structure FHAp. The *in vitro* test of 316LSS, HAp/316LSS and FHAp/316LSS materials in simulated body fluid (SBF) solution was realized with different immersion times. After 21 immersion days in SBF solution, the apatite crystals have a cactus-like shape, and they grow to form a thick block on the surface of FHAp/316LSS leading to the decrease of the corrosion current density during the immersion process in the SBF solution.

**Keywords:** 316LSS; electrodeposition; fluoridated hydroxyapatite coatings (FHAp); *in vitro* test; SBF.

## 1 Introduction

316L stainless steel (316LSS), titanium and alloys of titanium were widely used in orthopedic surgery, especially in dental technology because of their good mechanical properties, such as low elastic module, biocompatibility and corrosion resistance in the biological environment. In recent years, the demand for biomedical materials has increased, especially biomedical materials with a high quality. Therefore, a new research to improve the quality and biological compatibility with the human body of biomedical materials based on 316L stainless steel, titanium and titanium nitride by hydroxyapatite (HAp) coating seems to be the most investigated.

HAp has similar components to the mineral phase in natural bone and hard tissue of humans, so when it is implanted into the human body, it lead to faster bone healing and does not cause undesirable effects for the patient. HAp coatings on metal or alloy were synthesized by many different methods such as sol-gel, plasma spraying, chemical and electrochemical [1–4]. Indeed, the electrochemical deposition of HAp on metal or alloy surfaces has become an important technology for various applications due to both its ability to deposit on non-line-of-sight, porous or complex shapes of substrates and its availability and low cost of the equipment [5–9].

However, pure HAp coatings have relatively high solubility in the biological environment, especially HAp coatings which were made by the plasma spraying method, because the composition of the coatings contains a large amount of HAp amorphous phase. The high solubility can lead to decomposition of the coatings and prevent fixed ability of implant materials with the host tissue [5].

Fluorine is one of elements which exists in human bone and enamel; it can be incorporated into HAp crystal structure by replacing  $\text{OH}^-$  groups by  $F^-$  ions to form fluoridated hydroxyapatite (FHAp,  $\text{Ca}_{10}[\text{PO}_4]_6[\text{OH}]_{2-x}\text{F}_x$ , where  $0 < x < 2$  is the degree of fluoridation). Some studies have shown that FHAp has lower solubility than HAp, but it still maintains the bioactivity and biocompatibility. Recently, there have been many studies focusing on

\*Corresponding author: Dinh Thi Mai Thanh, Institute for Tropical Technology, Vietnam Academy of Science and Technology, 18 Hoang Quoc Viet, Cau Giay, Hanoi, Vietnam, e-mail: dmthanh@itt.vast.vn

Pham Thi Nam, Nguyen Thi Thom, Nguyen Thu Phuong, Vo Thi Hanh, Nguyen Thi Thu Trang and Vu Thi Hai Van: Institute for Tropical Technology, Vietnam Academy of Science and Technology, 18 Hoang Quoc Viet, Cau Giay, Hanoi, Vietnam

Trinh Hoang Trung: University of Science and Technology of Hanoi, Vietnam Academy of Science and Technology, 18 Hoang Quoc Viet, Cau Giay, Hanoi, Vietnam

Tran Dai Lam: Graduate University of Science and Technology, Vietnam Academy of Science and Technology, 18 Hoang Quoc Viet, Cau Giay, Hanoi, Vietnam



the application of FHAp coatings as bioactive and stable materials with longevity [5, 10–18].

This paper introduces synthesis results of FHAp coatings in a solution containing  $\text{Ca}^{2+}$ ,  $\text{H}_2\text{PO}_4^-$  and  $\text{F}^-$  by the cathode scanning potential method with different synthesis conditions, such as different concentrations of  $\text{F}^-$ ,  $\text{H}_2\text{O}_2$  and the different scanning potential ranges.

## 2 Materials and methods

### 2.1 Materials

316LSS samples (ASTM/A333, JSW. Ltd., Japan) [6] were 1 cm×10 cm size with a working area of 1 cm<sup>2</sup>. 316LSS samples were polished with P600 up to P1200 SiC grit papers (Japan), rinsed in distilled water and alcohol, and then dried at room temperature. All chemicals used in this paper are analytical reagent grade of Merck.

### 2.2 Synthetic conditions of FHAp coatings

FHAp coatings were synthesized on the 316LSS by the cathode scanning potential method with a scanning rate of 5 mV/s in 80 ml solution containing  $\text{Ca}^{2+}$ ,  $\text{H}_2\text{PO}_4^-$  and different concentrations of  $\text{F}^-$ . The solutions were denoted as follows:

SF0:  $3 \times 10^{-2}$  M  $\text{Ca}(\text{NO}_3)_2 \cdot 4\text{H}_2\text{O} + 1.8 \times 10^{-2}$  M  $\text{NH}_4\text{H}_2\text{PO}_4 + 0.15$  M  $\text{NaNO}_3 + 6\%$   $\text{H}_2\text{O}_2$  (wt/wt); SF1: SF0+0.001 M NaF; SF2: SF0+0.002 M NaF; and SF3: SF0+0.003 M NaF.

FHAp coatings were synthesized with different conditions. The different scanning potential ranges were: 0 to −0.8 V/SCE, −0.8 to −1.8 V/SCE, 0 to −1.6 V/SCE, 0 to −1.8 V/SCE and 0 to −2.5 V/SCE. The concentration of  $\text{H}_2\text{O}_2$  changes were 0%, 2%, 4%, 6% and 8% (wt/wt).

### 2.3 The determination of FHAp coating thickness

The mass of FHAp coatings deposited on the surface of 316LSS was determined by the mass of 316LSS samples before and after synthesis by a Precisa analytical balance (XR 205SM-PR, Swiss). The thickness of the coatings was calculated by the following equation:

$$\left. \begin{array}{l} D = \frac{m}{V} \\ V = S \cdot h \end{array} \right\} \rightarrow h = \frac{m}{D \cdot S} \quad (1)$$

$D = 3.13$  g/cm<sup>3</sup> is the specific mass of FHAp (approximation with the specific mass of HAp) [19]; the mass ( $m$ ) and volume ( $V$ ) of FHAp coatings;  $h$  is the thickness of FHAp coatings;  $S = 1$  cm<sup>2</sup> is the working area of the 316LSS cathode.

### 2.4 Coating characterization

The coating microstructure/morphology was characterized by scanning electron microscopy (SEM) using Hitachi S4800 equipment

(Japan). Fourier transform infrared (FTIR) spectra were recorded in the range of 4000–400 cm<sup>−1</sup>, with a resolution of 4 cm<sup>−1</sup> with a Nicolet 6700 spectrometer, using the KBr pellet technique. The spectra were the result of an accumulation of 32 scans. The composition of elements in FHAp coatings was determined by energy-dispersive X-ray spectroscopy (EDXS) on a JSM 6490-JED 1300 Jeol (Japan).

The phase purity and crystallinity of the FHAp coatings on the 316LSS were analyzed by X-ray diffraction (SIEMENS D5005 Bruker-Germany,  $\text{CuK}\alpha$  radiation ( $\lambda = 1.54056$  Å), with the following parameters: step angle of 0.030°, scanning rate of 0.04285°s<sup>−1</sup>, and  $2\theta$  in a range of 20–70°. The crystallite size of HAp and FHAp coatings was calculated from (002) reflection in X-ray diffraction (XRD) pattern, using Scherrer's equation [20]:

$$D = \frac{0.9\lambda}{B \cdot \cos\theta} \quad (2)$$

where  $D$  (nm) is crystallite size,  $\lambda$  is the wavelength of the X-ray radiation ( $\text{CuK}\alpha$ ),  $\theta$  (rad) is the diffraction angle, and  $B$  is the full width at half-maximum FWHM (rad) of the peak along (002) direction.

Lattice parameters ( $a$ ,  $c$ ) are calculated from peak (002) and (211) of XRD pattern according to Eq. (3), where,  $d$  is determined from XRD, which is the distance between adjacent planes in the set of Miller indices ( $hkl$ ) [21]:

$$\frac{1}{d^2} = \frac{4}{3} \frac{(h^2 + kh + k^2)}{a^2} + \frac{l^2}{c^2} \quad (3)$$

### 2.5 Preparation of simulated body fluid and *in vitro* test

A simulated body fluid (SBF) solution was used to perform the electrochemical behavior studies of 316LSS with and without HAp or FHAp coatings. The chemical composition of the SBF solution is shown in Table 1. The pH of the SBF solution was adjusted to 7.4 and the temperature was maintained at 37±1°C [22–24].

316LSS, HAp/316LSS and FHAp/316LSS samples limited to 1 cm<sup>2</sup> of active area were used as working electrodes and immersed in a three electrode cell containing 80 ml of SBF solution with a saturated calomel electrode (SCE) as a reference electrode and Pt foil as a counter electrode. The electrochemical cell was incubated at 37±1°C in a water bath during 21 days.

The working electrode was polarized in the potential range ±10 mV around its open circuit potential (OCP) with a scanning rate

**Table 1:** Chemical composition of the simulated body fluid (SBF) solution.

Compound	Content (g/l)
NaCl	8.00
KCl	0.40
CaCl <sub>2</sub>	0.18
NaHCO <sub>3</sub>	0.35
Na <sub>2</sub> HPO <sub>4</sub> ·2H <sub>2</sub> O	0.48
MgCl <sub>2</sub> ·6H <sub>2</sub> O	0.10
KH <sub>2</sub> PO <sub>4</sub>	0.06
MgSO <sub>4</sub> ·7H <sub>2</sub> O	0.10
Glucose	1.00



potential  $v=1$  mV/s. The polarization resistance  $R_p$  and the corrosion current  $I_{\text{corr}}$  were calculated from the Eqs. (4) and (5) with  $B=0.0203$  for 316LSS samples, 0.017 for HAp/316LSS samples and 0.016 for FHAp/316LSS (values determined from the Tafel slopes of the I-E curves with potential range  $\pm 150$  mV around its OCP from Eq. (6):

$$R_p = \frac{\Delta E}{\Delta i} \quad (4)$$

$$I_{\text{corr}} = \frac{B}{R_p} \quad (5)$$

$$B = \frac{b_a \cdot |b_c|}{2.3(b_a + |b_c|)} \quad (6)$$

where  $|b_c|$  is the absolute value of the cathodic Tafel slope and  $b_a$  is the value of the anodic Tafel slope.

The electrochemical impedance spectra (EIS Bode plots) vs. immersion time were carried out at OCP in the frequency range of  $10^6$  to  $10^{-2}$  Hz with 10 mV amplitude. Afterwards, the samples were rinsed with absolute alcohol and distilled water, then incubated at 25°C for 24 h for further analyses.

## 3 Results and discussion

### 3.1 Effect of $F^-$ concentration

The cathodic polarization curves of 316LSS substrate in electrolytes SF0, SF1, SF2 and SF3 are shown in Figure 1. Within the voltage range applied, several electrochemical reactions are suggested as follows [25]:

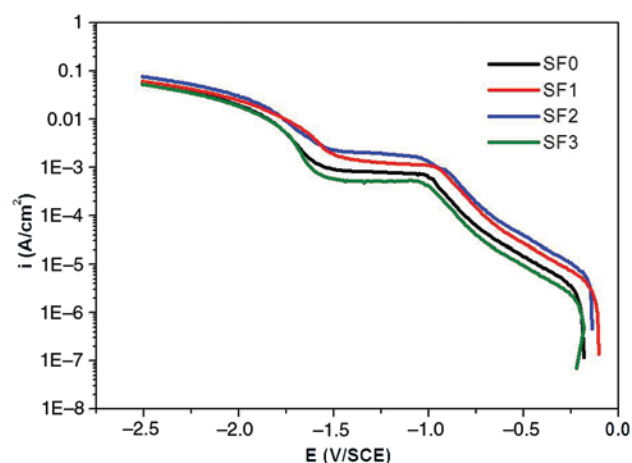
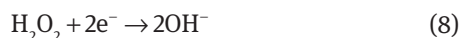
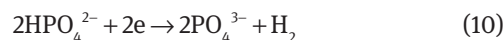
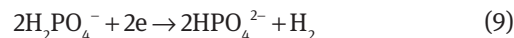
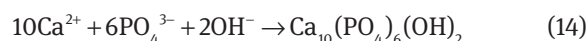
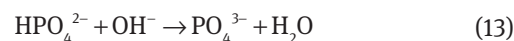
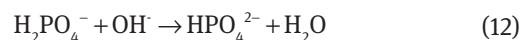


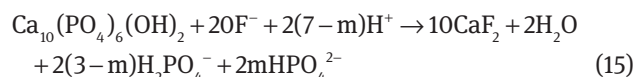
**Figure 1:** Cathodic polarization curves of 316LSS substrate in electrolytes SF0, SF1, SF2 and SF3.



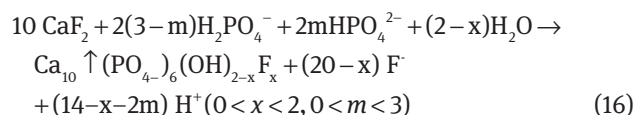
The formation of HAp coatings was observed on the surface of 316LSS. This can be explained as following:  $OH^-$  is generated on the 316LSS surface, and the pH value at the surrounding surface area of the cathode increased, leading to the formation of  $HPO_4^{2-}$  and  $PO_4^{3-}$  ions [Eqs. (12) and (13)]. Formation of HAp coatings occurs according to Eq. (14):



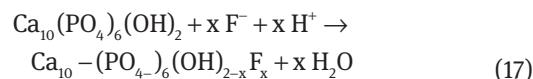
With the presence of  $F^-$  ions in electrolyte, the new reactions maybe occur. The first, the formation of  $CaF_2$  according to equation (15) [5]:



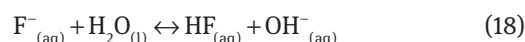
Then, the continuance reaction of  $CaF_2$  and  $HPO_4^{2-}$  or  $H_2PO_4^-$  happens, to form FHAp:



Eqs. (15) and (16) showed the formation mechanism of FHAp coatings by the cathode precipitate method as follows:



The polarization curves of the 316LSS electrode in electrolytes SF0, SF1 and SF2 showed that the cathode current density increased when the concentration of  $F^-$  increased from 0 M to 0.002 M. The cathode current density decreased with the electrolyte containing 0.003 M  $F^-$  (SF3). This decrease is explained by the fact that when the concentration of  $F^-$  increased, this led to the concentration of  $OH^-$  ion being increased according to Eq. (18). This increase inhibited the reactions which generated  $OH^-$  on the cathode electrode such as: the reduction reactions of  $O_2$  (7),  $H_2O_2$  (8) and  $H_2O$  (11).





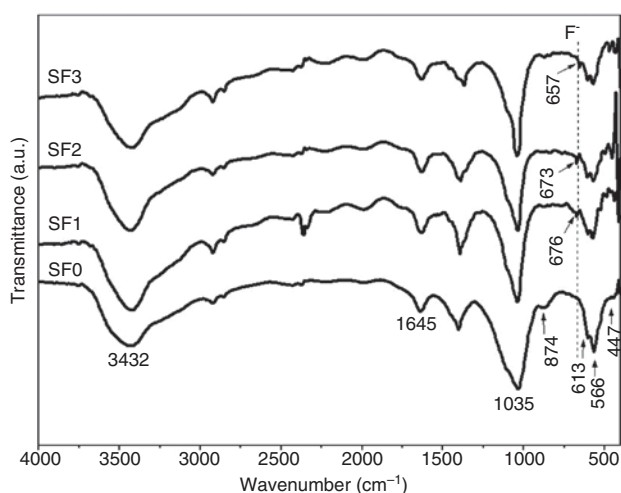
The variation of the coating mass and the thickness of FHAp synthesized in the solutions with different concentrations of  $F^-$  (0 M, 0.001 M, 0.002 M and 0.003 M) with the potential range from 0 to  $-1.8$  V/SCE, for 30 min (5 scans) at  $25^\circ\text{C}$  is shown in Table 2. When the concentrations of  $F^-$  ions increased from 0 M to 0.002 M, the mass of FHAp coatings increased from  $1.9\text{ mg/cm}^2$  to  $3.0\text{ mg/cm}^2$ , respectively. However, when the concentration of  $F^-$  was 0.003 M, the mass of FHAp coatings was only  $2.1\text{ mg/cm}^2$ , which decreased in comparison with the sample synthesized in SF2 solution. The coating thickness according to Eq. (1) was the largest ( $9.6\text{ }\mu\text{m}$ ) at 0.002 M  $F^-$ . Thus, the SF2 solution was chosen for the next studies.

Figure 2 shows the IR spectra in the wave number range from  $4000\text{ cm}^{-1}$  to  $400\text{ cm}^{-1}$  of FHAp coatings which were synthesized in SF0, SF1, SF2 and SF3 solutions. The results showed the characteristic peaks of HAp such as  $\text{PO}_4^{3-}$  and  $\text{OH}^-$ . The peaks of  $\text{PO}_4^{3-}$  group were observed at  $1035\text{ cm}^{-1}$ ,  $613\text{ cm}^{-1}$ ,  $566\text{ cm}^{-1}$  and  $447\text{ cm}^{-1}$ ; the vibrations of  $\text{OH}^-$  were observed at  $3432\text{ cm}^{-1}$  and  $1645\text{ cm}^{-1}$ . Moreover, in the IR spectra we also observed a new peak at  $676\text{ cm}^{-1}$  (SF1),  $673\text{ cm}^{-1}$  (SF2) and  $657\text{ cm}^{-1}$  (SF3) which characterized the vibration of  $F^-$ .

**Table 2:** The variation of the mass and the thickness of fluoridated hydroxyapatite (FHAp) coatings synthesized in the solutions with the different concentrations of  $F^-$ .

Electrolyte	SF0	SF1	SF2	SF3
FHAp mass ( $\text{mg/cm}^2$ )	1.9	2.7	3	2.1
Thickness ( $\mu\text{m}$ )	6.1	8.6	9.6	6.7

FHAp, Fluoridated hydroxyapatite.



**Figure 2:** IR spectra of fluoridated hydroxyapatite (FHAp) coatings synthesized in the solutions: SF0, SF1, SF2 and SF3.

These results have a good agreement with the literature data by other researchers [5].

Figure 3 presents the XRD patterns of HAp and FHAp coatings synthesized in SF0 and SF2 solution. Both XRD patterns exhibit the HAp phase. The typical peaks were found at  $2\theta$  of  $32^\circ$  (211) and  $26^\circ$  (002). These results show that FHAp coating was crystals and single phase of HAp.

The diameter of the crystals was calculated according to Scherrer formula (Eq. 2). Crystal diameter of FHAp coating was about  $104\text{ nm}$ . It was smaller than that of HAp ( $106\text{ nm}$ ). This can be explained by the radius of  $F^-$  ions ( $1.36\text{ }\text{\AA}$ ) which was smaller than  $\text{OH}^- \sim \text{O}^{2-} = 1.40\text{ }\text{\AA}$ . When the  $\text{OH}^-$  group was replaced by the  $F^-$  ion, crystal size was reduced.

Table 3 presents distance between the planes of the crystal ( $d$ ) at two planes (002) and (211) and the value of the lattice constant  $a$ ,  $b$ ,  $c$  of FHAp. These values of HAp and FHAp are lower in comparison with NIST standard of the HAp sample [26]. This result shows that  $F^-$  ions incorporated into the HAp lattice structure.

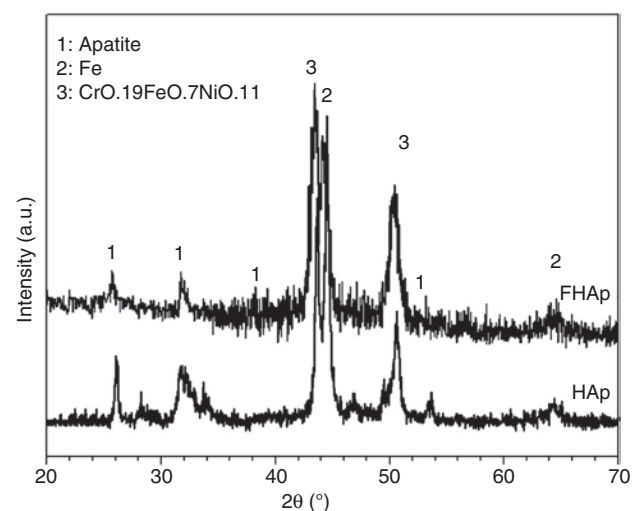


**Figure 3:** X-ray diffraction (XRD) patterns of hydroxyapatite (HAp)/316LSS and fluoridated hydroxyapatite (FHAp)/316LSS synthesized in SF0, SF2 solution.

**Table 3:** Values of distance between the planes of the crystal  $d(002)$ ,  $d(211)$  and the value of the lattice constant ( $a$ ,  $b$ ,  $c$ ) of fluoridated hydroxyapatite (FHAp).

	NIST (HAp) [26]	HAp	FHAp
$d(002)$	3.44	3.438	3.436
$d(211)$	2.82	2.815	2.813
$a=b$ ( $\text{\AA}$ )	9.4451	9.4261	9.41915
$c$ ( $\text{\AA}$ )	6.88	6.876	6.872

HAp, Hydroxyapatite; FHAp, fluoridated hydroxyapatite.



The components of FHAp coatings obtained with the variation of  $F^-$  in the synthesis solution: 0 M, 0.001 M, 0.002 M and 0.003 M were analyzed by the EDX spectra (Figure 4). The results showed the presence of four main elements in the components of FHAp: O, F, P and Ca. In addition, there was the presence of the elements: Na, Cl, Si, S, Cr, Ni and Fe. The presence of Na was explained by the fact that the synthesis solutions contained the salts of NaF and  $NaNO_3$ . The elements Si, S, Cr, Ni and Fe presented in EDX spectra because they were the component elements of 316LSS. Finally, the diffusion of KCl from the SCE electrode into the synthesis solution is the cause of the presence of Cl.

In the solution SF0 (without  $F^-$ ), the contents of O, P and Ca are 35.64%, 16.66% and 27.74%, respectively. The ratio of Ca/P is 1.3, which is lower than that of natural bone.

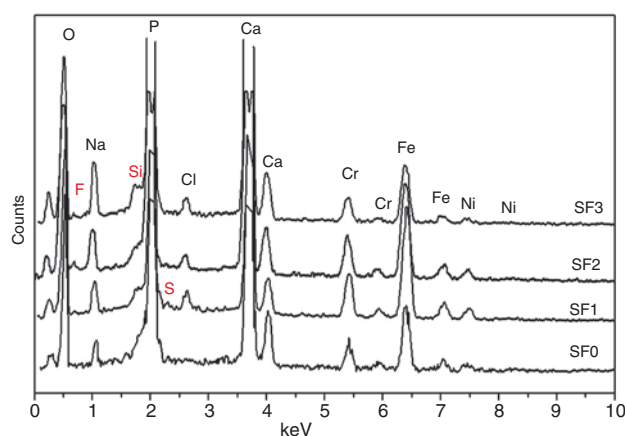


**Figure 4:** The energy-dispersive X-ray (EDX) spectra of fluoridated hydroxyapatite (FHAp)/316LSS synthesized in the solutions: SF0, SF1, SF2 and SF3.

With the increase in concentration of  $F^-$  in the synthesis solution from 0 M to 0.002 M, the content of  $F^-$  in FHAp coatings increased from 0% to 1.7%. With 0.003 M  $F^-$  in the synthesis solution, the content of  $F^-$  in FHAp coatings was 1.27% (Table 4). In the solutions SF1, SF2, SF3, the ratio of Ca/P is lower than in SF0 solution and these values are lower than 1.67. These results may be due to the influence of the elements in the SCE electrode, electrolyte and 316LSS substrate.

The numbers of  $OH^-$  groups in HAp crystals were replaced by  $F^-$  ions which can be calculated by the content of  $F^-$  in FHAp coatings. We can calculate the ratio of F/Ca to give the formula of FHAp (Table 5). The F/Ca maximum ratio in the coating is 0.143; the formula of FHAp was  $Ca_{10}(PO_4)_6(OH)_{2-1.43}F_{1.43}$ .

### 3.2 Effect of the scanning potential range

FHAp coatings were synthesized in SF2 solution with different potential ranges: 0 to  $-0.5$  V/SCE, 0 to  $-0.8$  V/SCE, 0 to  $-1.6$  V/SCE, 0 to  $-1.8$  V/SCE,  $-0.8$  to  $-1.8$  V/SCE and 0 to  $-2.5$  V/SCE, at  $25^\circ\text{C}$ ,  $\text{pH}=4.3$ , five scans, scanning rate of 5 mV/s. Table 6 shows the mass of FHAp coatings formed on 316LSS with the different potential ranges. The results showed that FHAp coatings were not formed when the potential range was from 0 V/SCE to  $-0.5$  V/SCE. When the potential range was larger, the mass of FHAp coatings increased and reached the maximum value at  $5.5 \text{ mg/cm}^2$  (at the potential range 0 V/SCE to  $-1.8$  V/SCE). However, the mass of coating decreased ( $3.9 \text{ mg/cm}^2$ ) when the potential range was 0 V/SCE to  $-2.5$  V/SCE. The decrease of the mass was explained as follows: with the large scanning potential range, further increase in the amount of  $OH^-$  and  $PO_4^{3-}$  ions on the electrode surface led to their

**Table 4:** The component of elements of fluoridated hydroxyapatite (FHAp) synthesized on 316LSS in the solutions SF0, SF1, SF2 and SF3.

Elements	% mass				% atomic			
	SF0	SF1	SF2	SF3	SF0	SF1	SF2	SF3
O	35.64	30.72	32.65	35.26	57.55	52.87	53.35	55.26
P	16.66	14.54	15.64	16.13	13.89	12.92	13.20	13.13
Ca	27.74	20.01	25.12	25.40	17.88	13.75	16.38	15.99
F	–	0.76	1.70	1.27	–	1.1	2.34	1.69
Na	2.08	3.02	4.05	4.73	2.34	3.62	4.61	5.19
S	–	0.27	–	–	–	0.24	–	–
Si	–	–	–	0.73	–	–	–	0.66
Cl	–	0.87	0.97	0.82	–	0.68	0.72	0.55
Cr	3.22	5.88	4.11	3.08	1.60	3.11	2.07	1.50
Fe	13.08	20.91	13.92	11.41	6.05	10.31	6.51	5.16
Ni	1.58	3.01	1.83	1.16	0.69	1.41	0.82	0.50



**Table 5:** The formula of fluoridated hydroxyapatite (FHAp) based on the content of F<sup>-</sup>.

Solution	% mass of F <sup>-</sup>	F/Ca	The formula of FHAp $\text{Ca}_{10}(\text{PO}_4)_6(\text{OH})_{2-x}\text{F}_x$
SF0	0	0	$\text{Ca}_{10}(\text{PO}_4)_6(\text{OH})_2$
SF1	0.76	0.08	$\text{Ca}_{10}(\text{PO}_4)_6(\text{OH})_{2-0.8}\text{F}_{0.8}$
SF2	1.7	0.143	$\text{Ca}_{10}(\text{PO}_4)_6(\text{OH})_{2-1.43}\text{F}_{1.43}$
SF3	1.27	0.106	$\text{Ca}_{10}(\text{PO}_4)_6(\text{OH})_{2-1.06}\text{F}_{1.06}$

FHAp, Fluoridated hydroxyapatite.

**Table 6:** The variation of mass and the thickness of fluoridated hydroxyapatite (FHAp) according to the different scanning potential ranges.

Scanning potential range (V/SCE)	Mass (mg/cm <sup>2</sup> )	Thickness (μm)
0 to -0.5	0	0
0 to -0.8	$5.10 \times 10^{-4}$	$1.6 \times 10^{-3}$
0 to -1.6	1.55	5
-0.8 to -1.8	5	9.6
0 to -1.8	5.5	17.6
0 to -2.5	3.9	12.5

diffusion from the electrode surface into the solution and these ions combined with Ca<sup>2+</sup> and F<sup>-</sup> to form FHAp in the solution. Simultaneously, with the large cathode potential, reduction of the solvent is promoted, and thus the formation of hydrogen bubbles on the electrode surface may reduce the adhesion ability of FHAp coatings with the 316LSS substrate. So, the suitable potential range is 0 V/SCE to -1.8 V/SCE.

The variation of the coating thickness with the different scanning potential ranges was calculated according to Eq. (1) (Table 6). The thickness of FHAp coatings increased with increasing of the scanning potential range and the maximum was 17.6 μm with the scanning potential range from 0 V/SCE to -1.8 V/SCE.

SEM images of FHAp/316LSS coating synthesized in SF2 solution with the various scanning potential ranges are presented in Figure 5. The results show that the scanning potential range affected morphology of FHAp coating. Rod shapes with average size of about 100–300 nm of FHAp were observed when they were synthesized at the scanning potential ranges 0 to -0.8 V/SCE, 0 to -1.8 V/SCE and 0 to -2.5 V/SCE. With the scanning potential range from 0 V/SCE to -1.6 V/SCE, FHAp coating had a spherical shape with average diameter about 100 nm. A flake-like shape was observed when FHAp was synthesized at the scanning potential range from -0.8 V/SCE to -1.8 V/SCE.

### 3.3 Effect of H<sub>2</sub>O<sub>2</sub>

Synthesis process of FHAp coatings by the cathodic scanning potential method always happens simultaneously with H<sub>2</sub>O reduction to generate H<sub>2</sub>, this reaction will consume a huge electric power leading to a high cost to synthesize FHAp coatings. By contrast, the generation of H<sub>2</sub> will make FHAp coatings highly porous, so the adhesion with the substrate decreases. H<sub>2</sub>O<sub>2</sub> is a strong oxidation agent, can replace for the water in the reduction reaction on the cathode to generate OH<sup>-</sup> ions [Eq. (8)], thus favoring the chemical reactions leading to the formation of FHAp [4].

To select a suitable H<sub>2</sub>O<sub>2</sub> concentration for the synthesis process of FHAp coatings on 316LSS by the scanning potential method, the cathodic polarization curves of 316LSS electrode in SF2 solution with various H<sub>2</sub>O<sub>2</sub> concentrations [0%, 2%, 4%, 6% and 8% H<sub>2</sub>O<sub>2</sub> (wt/wt)] at 25°C were recorded (Figure 6). In general, all the curves have the same shape. However, the cathodic current density decreases with addition of H<sub>2</sub>O<sub>2</sub> in the synthesis solution. This can be explained by the fact that when the synthesis potential ranges from 0 V/SCE to -1.8 V/SCE, which is convenient for formation of FHAp, the water electrolysis also happens, generating more OH<sup>-</sup> leading to current density increases. With a small H<sub>2</sub>O<sub>2</sub> concentration (<2%) in electrolyte, the water reduction is reduced, so the cathode current density decreases. However, the H<sub>2</sub>O<sub>2</sub> concentration from 4% to 8% is large enough for the rising of cathodic current density. However, when the concentration of H<sub>2</sub>O<sub>2</sub> is 8%, leading to a huge amount of OH<sup>-</sup> surrounding the cathode surface, FHAp does not only form on the surface of the electrode, but also forms in the solution in the area around cathode; this phenomenon can be seen with the white FHAp precipitate in the bottom of the cell.

Figure 7 presents the variation of FHAp coating mass with the changing the concentration of H<sub>2</sub>O<sub>2</sub>. The result shows that the mass of synthesis FHAp coatings increases from 3.25 mg/cm<sup>2</sup> to 5.1 mg/cm<sup>2</sup> with the H<sub>2</sub>O<sub>2</sub> concentration from 0% to 6%. With the continuous rise of concentration of H<sub>2</sub>O<sub>2</sub> to 8%, the mass of FHAp coatings decreases to 3.05 mg/cm<sup>2</sup>. This can be explained by the fact that the amount of OH<sup>-</sup> formation in electrode surface diffuses into the electrolyte and forms FHAp in the solution, leading to the mass reducing greatly. H<sub>2</sub>O<sub>2</sub> concentration at 6% gives the most uniform and good adhesion FHAp coatings. So, 6% H<sub>2</sub>O<sub>2</sub> is chosen for the FHAp coatings synthesis process by the electrochemical method. With the FHAp mass of 5.1 mg/cm<sup>2</sup> at 6% H<sub>2</sub>O<sub>2</sub>, the FHAp coating thickness is 16.3 μm, following Eq. (1).



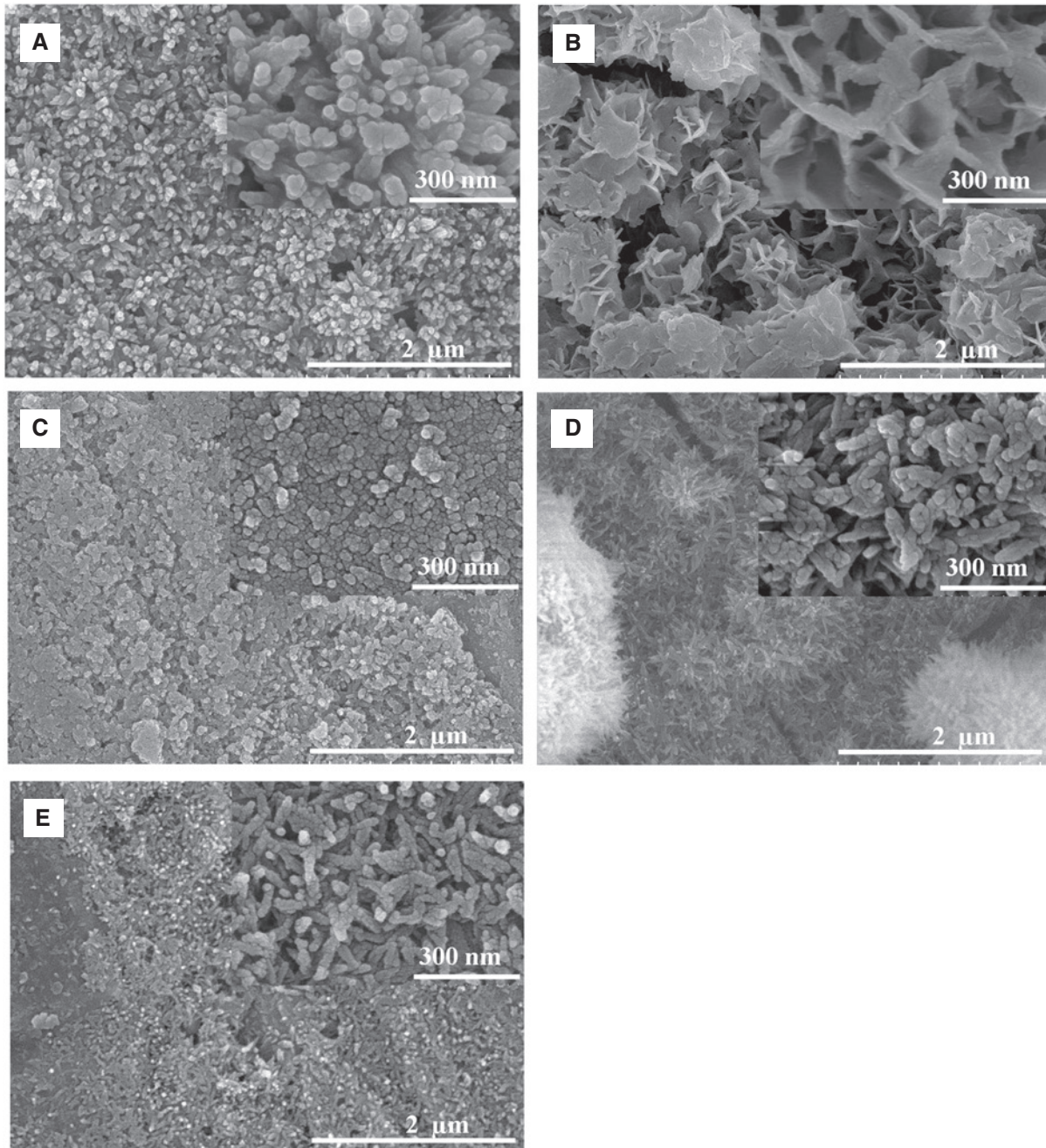


**Figure 5:** Scanning electron microscopy (SEM) images of fluoridated hydroxyapatite (FHAp)/316LSS coatings synthesized at various potential ranges: (A) 0 V/SCE to  $-0.8$  V/SCE; (B)  $-0.8$  V/SCE to  $-1.8$  V/SCE; (C) 0 V/SCE to  $-1.6$  V/SCE; (D) 0 V/SCE to  $-1.8$  V/SCE and (E) 0 V/SCE to  $-2.5$  V/SCE.

### 3.4 *In vitro* test

When metal and alloy materials are used as implants in the body, they can be corroded [27, 28]. This can result in weakness of the implants and/or release of undesired and harmful corrosion products to the surrounding tissue [29, 30]. In order to investigate the behavior of HAp and FHAp coatings in corrosion media, corrosion tests were carried out.

#### 3.4.1 The polarization resistances

The variation of the polarization resistances ( $R_p$ ) and the corrosion current density ( $i_{\text{corr}}$ ) which extrapolated from the Tafel polarization curves vs. time of 316LSS without and with HAp or FHAp in SBF solution follows Eqs. (4) and (5), as shown in Figure 8. The result shows that the  $R_p$  of HAp or FHAp coated 316LSS is always higher than



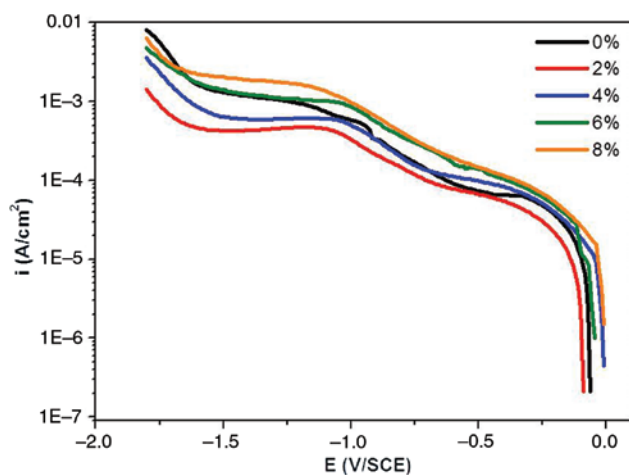


**Figure 6:** Cathodic polarization curves of 316LSS electrode in SF<sub>2</sub> solution with various H<sub>2</sub>O<sub>2</sub> concentrations 0% to 8%.

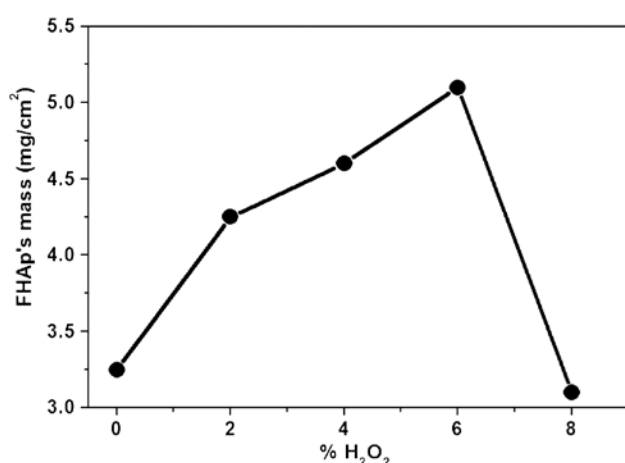


**Figure 7:** The variation of fluoridated hydroxyapatite (FHAp) mass vs. H<sub>2</sub>O<sub>2</sub> concentration.

uncoated 316LSS during immersion in SBF and the  $R_p$  of FHAp/316LSS is higher than HAp/316LSS, about 1.4 times, after 21 immersion days. The  $i_{corr}$  has the opposite change rule with  $R_p$ . The result shows that the uncoated 316LSS is corroded with an  $i_{corr}$  value higher than 3  $\mu\text{A}/\text{cm}^2$  for any time, but it decreases about two to three times with HAp or FHAp coated 316LSS. These results confirm that the ability to protect the substrate of coatings and FHAp is better than HAp coating.

### 3.4.2 Electrochemical impedance

To confirm the results obtained from polarization tests during immersion in the SBF solution, electrochemical impedance measurements were further recorded at OCP.

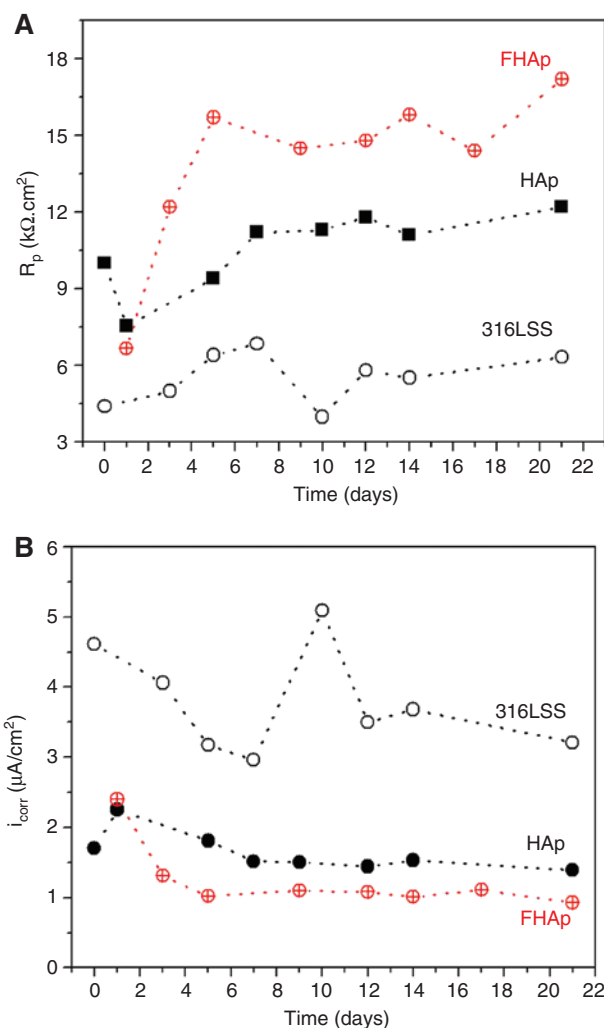


**Figure 8:** The variation of  $R_p$  (A) and  $i_{corr}$  (B) of 316LSS, hydroxyapatite (HAp)/316LSS and fluoridated hydroxyapatite (FHAp)/316LSS vs. different immersion times in simulated body fluid (SBF) solution.

Figure 9 shows Bode plots of 316LSS, HAp/316LSS and FHAp/316LSS vs. different immersion times in the SBF solution. For 316LSS, impedance increases continuously during 21 days of immersion. With the HAp/316LSS sample, the first time, impedance is much higher than 316LSS because of the protection ability of HAp coating, but following the immersion period, impedance increases and decreases, and is lower than the beginning; this can be explained by the fact that the rate of HAp dissolution is faster than HAp formation. The impedance of FHAp/316LSS increases and decreases slightly and is almost stable during the immersion period.

To see the variation of the impedance of apatite coatings which formed on 316LSS, HAp/316LSS and FHAp/316LSS, the impedance modulus at 1 Hz with different immersion times was determined (Figure 10). The



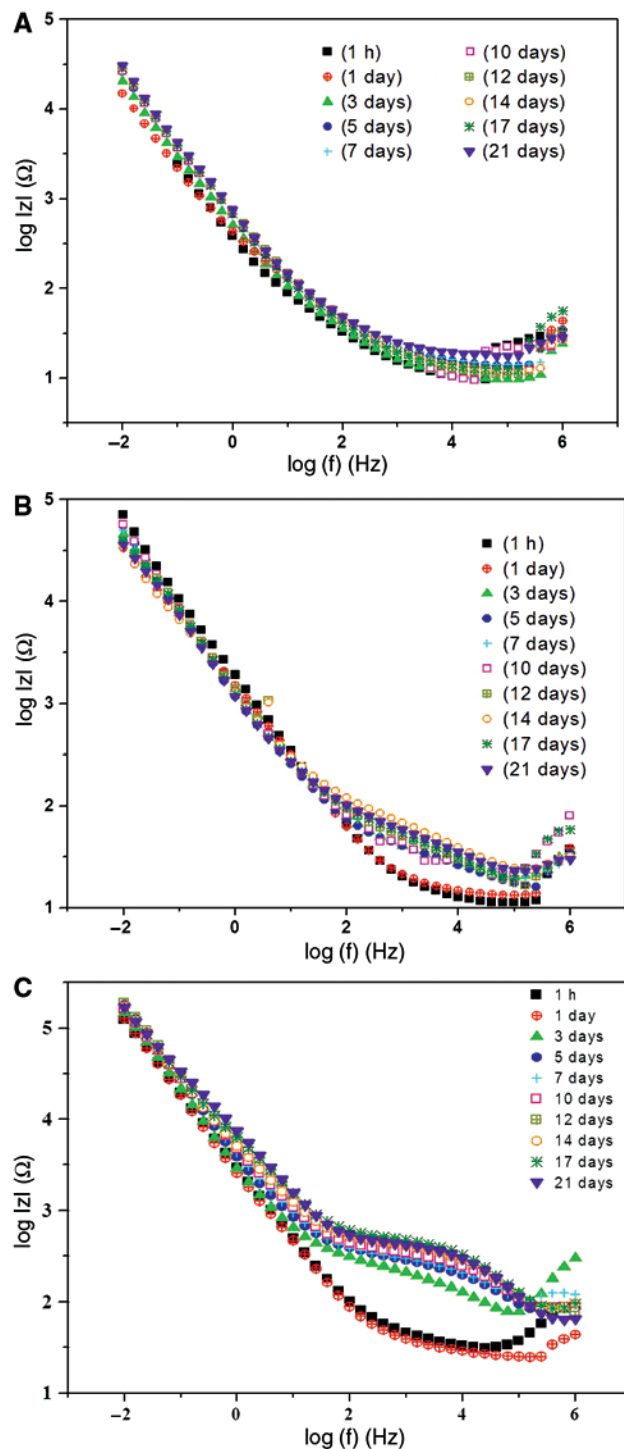


**Figure 9:** Bode impedance plots of 316LSS (A), hydroxyapatite (HAp)/316LSS (B), fluoridated hydroxyapatite (FHAp)/316LSS (C) vs. immersion time in simulated body fluid (SBF).

value of impedance modulus at the frequency 1 Hz characterizes the changing process of the apatite coatings formation on 316LSS and the precipitation and dissolution of apatite for HAp/316LSS and FHAp/316LSS samples.

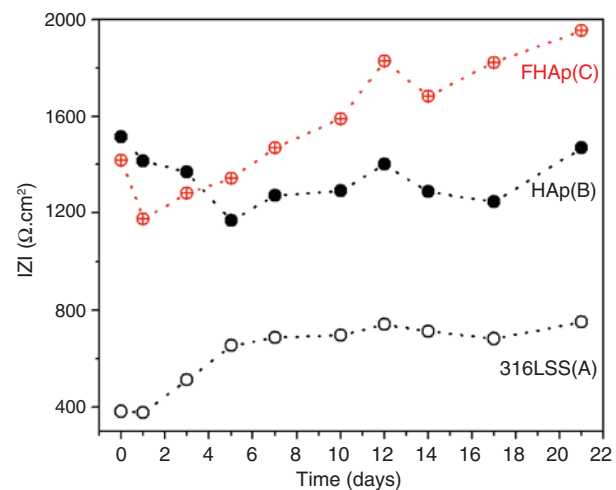


**Figure 10:** The variation of impedance modulus at 1 Hz of 316LSS (A), hydroxyapatite (HAp)/316LSS (B) and fluoridated hydroxyapatite (FHAp)/316LSS (C) versus immersion time in simulated body fluid (SBF).

The impedance modulus of 316LSS has an increasing trend during the immersion time and is about 751  $\Omega \cdot \text{cm}^2$  after 21 days. For HAp/316LSS, the impedance modulus fluctuates at different immersion times. It decreases continuously from 1515  $\Omega \cdot \text{cm}^2$  to 1168  $\Omega \cdot \text{cm}^2$  (1 and 5 immersion days, respectively) and increases at 12 days, then decreases at 17 days. This value increases again to 1468  $\Omega \cdot \text{cm}^2$  after 21 immersion days. About FHAp/316LSS, the impedance modulus has a value of 1418  $\Omega \cdot \text{cm}^2$  at the beginning. In 1 day, it decreases then increases continuously to 1827  $\Omega \cdot \text{cm}^2$  in 12 days. With 14 immersion days, the impedance modulus decreases and increases again to 1953  $\Omega \cdot \text{cm}^2$  after 21 days.

The increase or decrease of the impedance modulus of HAp/316LSS and FHAp/316LSS exhibits the formation and/or the dissolution of HAp and FHAp coatings that happen simultaneously in the immersion process.

In general, after 21 immersion days, the impedance modulus at 1 Hz frequency of FHAp/316LSS has a higher value than 316LSS and HAp/316LSS. This result shows that the protection ability for the substrate of FHAp coating is better than that of HAp coating in SBF solution.

### 3.4.3 SEM images

Figure 11 presents SEM images of 316LSS, HAp/316LSS and FHAp/316LSS before and after 21 immersion days in SBF solution. After immersion, the formation of new apatite crystals is observed on the surface of all materials. With



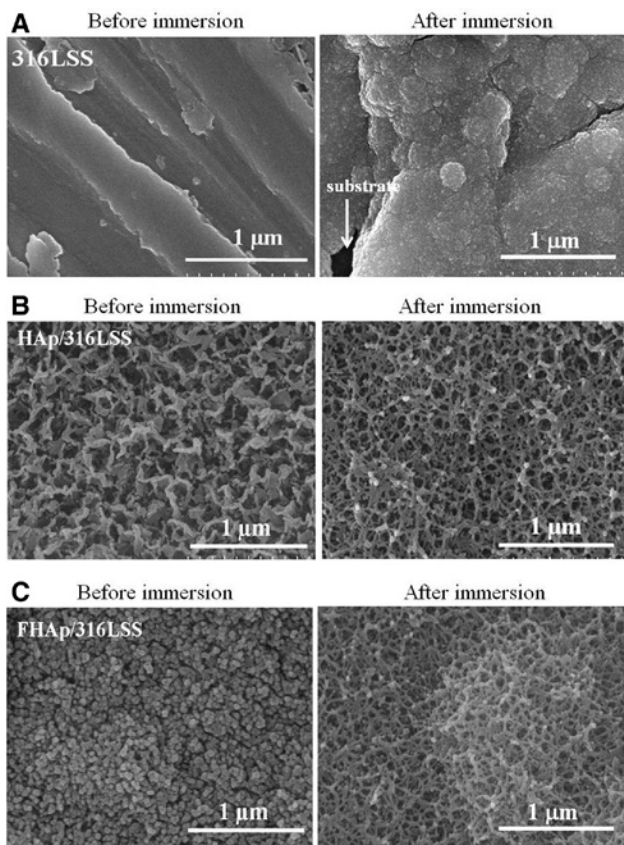


**Figure 11:** Scanning electron microscopy (SEM) images of 316LSS, hydroxyapatite (HAp)/316LSS and fluoridated hydroxyapatite (FHAp)/316LSS before and after 21 immersion days in simulated body fluid (SBF) solution.

the 316LSS substrate after immersion in the SBF solution, sphere shape crystals of apatite are formed and do not fully cover its surface. Before immersion, the morphology of HAp/316LSS has a cactus-like shape, while FHAp/316LSS has a rod shape. After 21 immersion days in SBF solution, with both HAp and FHAp coated materials, the formed apatite has a cactus-like shape and grows to form a thick block on the surface.

## 4 Conclusions

FHAp coatings were successfully synthesized on the 316LSS surface by the electrodeposition method via a simple technique. The optimal conditions were determined as follows: the electrolyte  $3 \times 10^{-2}$  M  $\text{Ca}(\text{NO}_3)_2 \cdot 4\text{H}_2\text{O}$  +  $1.8 \times 10^{-2}$  M  $\text{NH}_4\text{H}_2\text{PO}_4$  + 0.15 M  $\text{NaNO}_3$  + 6%  $\text{H}_2\text{O}_2$  + 0.002 M NaF, at 25°C, and the scanning potential range from 0 V/SCE to -1.8 V/SCE during five scans and 5 mV/s. The obtained coatings were single phase crystals of HAp, with a rod

shape and average size 100 nm×30 nm. The highest content of the  $\text{F}^-$  ion is 1.7% and the molecular formula  $\text{Ca}_{10}(\text{PO}_4)_6(\text{OH})_{2-1.43}\text{F}_{1.43}$ . *In vitro* tests in SBF were carried out and then the morphological changes were estimated by SEM. The protection ability for 316LSS substrate of HAp and FHAp coating was investigated by polarization and impedance measurements. It was also found that the occurrence of two processes (dissolution and formation of HAp or FHAp on the surface) should be discussed deeply in order to produce good implant materials with the desired properties and characteristics.

**Acknowledgments:** This work was supported by the Vietnam Academy of Science and Technology (VAST) (under grant no. VAST.ΔLT.01/15-16) and the Hanoi Department of Science and Technology (under grant no. 01C-03/01-2015-2).

## References

- [1] Yung CY, Edward C. *Surf. Coat. Technol.* 2005, 190, 122–131.
- [2] Qiuhua Y, Teresa DG. *Thin Solid Films* 2009, 518, 55–60.
- [3] Andrei VS, Samuel H. *Surf. Coat. Technol.* 2007, 202, 1236–1241.
- [4] Dong YL, Xiao XW. *Surf. Coat. Technol.* 2010, 204, 3205–3213.
- [5] Jian W, Yonglie C, Qianbing W, Zhimin Z, Haiyang Y. *Acta Biomater.* 2009, 5, 1798–1807.
- [6] Thanh DTM, Nam PT, Phuong NT, Que LX, Anh NV, Hoang T, Lam TD. *Mater. Sci. Eng. C* 2013, 33, 2037–2045.
- [7] Wang H, Eliaz N, Xiang Z, Hsu HP, Spector M, Hobbs LW. *Biomaterials* 2006, 27, 4192–4203.
- [8] Eliaz N, Eliyahu M. *J. Biomed. Mater. Res. A* 2007, 80, 621–634.
- [9] Eliaz N, Sridhar TM. *Cryst. Growth Des.* 2008, 8, 3965–3977.
- [10] Sivakumar M, Manjubala I. *Mater. Lett.* 2001, 50, 199–205.
- [11] Cavalli M, Gnappi G, Montenero A, Bersani D, Lottici PP, Laciulis S. *J. Mater. Sci.* 2001, 36, 3253–3260.
- [12] Zhang S, Xianting Z, Yongsheng W, Kui C, Wenjian W. *Surf. Coat. Tech.* 2006, 200, 6350–6354.
- [13] Baronov SM, Tumanov SV, Fadeeva IV, Bibikov VY. *Inorg. Mater.* 2003, 39, 877–880.
- [14] Lee EJ, Lee SH, Kim HW, Kong YM, Kim HE. *Biomaterials* 2005, 26, 3843–3851.
- [15] Kim HW, Kong YM, Bea CJ, Noh YI, Kim HE. *Biomaterials* 2004, 25, 2919–2929.
- [16] Cheng K, Weng W, Qu H, Du P, Shen G, Han G. *J. Biomed. Mater. Res. B* 2004, 69, 33–37.
- [17] Qu H, Wei M. *Acta Biomater* 2006, 2, 113–119.
- [18] Kim HW, Kim HE, Knowles JC. *Biomaterials* 2004, 25, 3351–3358.
- [19] Chen Y, Miao X. *Biomaterials* 2005, 26, 1205–1210.
- [20] Manara S, Paolucci F, Palazzo B, Marcaccio M, Foresti E, Tosi G, Sabbatini S, Sabatino P, Altankov G, Roveri N. *Inorg. Chim. Acta* 2008, 361, 1634–1645.
- [21] Thomas JW, Elizabeth AMS, Jennifer LS, Elliot BS. *Biomaterials* 2004, 25, 2111–2121.
- [22] Alves VA, Reis RQ, Santos ICB, Souza DG, Goncalves TF, Silva MAP, Rossi A, Silva LA. *Corros. Sci.* 2009, 51, 2473–2482.



- [23] Nath S, Tu R, Goto T. *Surf. Coat. Technol.* 2011, 206, 172–177.
- [24] Tamilselvi S, Raman V, Rajendran N. *Electrochim. Acta* 2006, 52, 839–846.
- [25] Kuo MC, Yen SK. *Mater. Sci. Eng. C* 2002, 20, 153–160.
- [26] Watters RL. *Calcium Hydroxyapatite (Certificate of Analysis, Standard Reference Material 2910a)*. Institute of Standards and Technology, NIST Measurement Services Division National: Gaithersburg, MD, 2008.
- [27] French HG, Cook SD, Haddad RJ. *J. Biomed. Mater. Res.* 1984, 18, 817–828.
- [28] Davies JE, Lowenberg B, Shiga A. *J. Biomed. Mater. Res.* 1990, 24, 1289–1306.
- [29] Michel R. *Crit. Rev. Biocompat.* 1987, 3, 235–317.
- [30] Finnegan M. *Crit. Rev. Biocompat.* 1989, 5, 1–11.

**Nguyen Thu Phuong**

Nguyen Thu Phuong received her MSc in Theoretical and Physical Chemistry from Hanoi University of Education in 2010. Since 2010, she has been a researcher at the Department of Corrosion and Protection of Metals, ITT, VAST. Her present researches concern metal organic framework and biomedical materials.

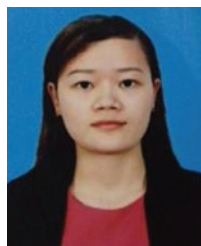
## Bionotes

**Pham Thi Nam**

Pham Thi Nam has worked as a researcher at Institute for Tropical Technology (ITT), Vietnam Academy of Science and Technology (VAST) since 2010. She has published more than 20 articles and reports in national and international journals related to  $\text{PbO}_2$  and hydroxyapatite (HAp). In the past 5 years, her PhD student project has worked in the field of electrodeposition of HAp coating which is applied in the biomedical.

**Vo Thi Hanh**

Vo Thi Hanh received her MSc in Theoretical and Physical Chemistry from Hanoi University of Education in 2006. Since 2007, she has been a lecturer at Hanoi University of Mining and Geology, and since 2014, she has been a PhD student at the Department of Corrosion and Protection of Metals, ITT, VAST, with concerns of hydroxyapatite coating.

**Nguyen Thi Thom**

Nguyen Thi Thom received her MSc in theoretical and physical chemistry from Hanoi University of Education in 2013. Since 2014, she has been a researcher at the Department of Corrosion and Protection of Metals, ITT, VAST. She has been studying for her PhD since 2015. Her present researches are synthesis of nanocomposite HAp/CNT coatings on biomedical alloys.

**Nguyen Thi Thu Trang**

Nguyen Thi Thu Trang worked as a Researcher at ITT, VAST. She received her MSc in chemistry from Vietnam National University of Hanoi, in 2005. Nearly 30 of her articles and reports related to conducting polymers and polymer nanocomposites have been published in national journals, international journals and proceedings of workshops.



**Vu Thi Hai Van**

Vu Thi Hai Van received her Bachelor's degree in chemistry from Hanoi National University of Education in 2013. She has researched about HAp and fluoridated hydroxyapatite (FHAp). She is now a PhD student in the field of nanocomposites in corrosion and protection metal.

**Trinh Hoang Trung**

Trinh Hoang Trung obtained his bachelor's degree in Hanoi University of Pharmacy in 2014, specializing in Clinical Pharmacy. Now, he is studying in Hanoi University of Science and Technology, in a Master 2 training course, department of Biology/Pharmacology.

**Tran Dai Lam**

Tran Dai Lam received his PhD in Physical Chemistry from the University of Paris VII, Paris, France, in 2003. He worked at Hanoi University of Technology and Institute of Materials Science. Now, he works at the Graduate University of Science and Technology, VAST and his research is related to nanobiomaterials for application in drug delivery systems and biosensors.

**Dinh Thi Mai Thanh**

Dinh Thi Mai Thanh received her PhD from the University of Paris 6, France, in 2003. Beginning in 1994, she was an assistant Researcher at the Department of Corrosion and Protection of Metals, ITT, VAST. Since 2010, she has been an Associate Professor at ITT. Her current research interests include nanofabrication, characterization and application in bone implants.